Journal of Computer Science and Artificial Intelligence
ISSN: 3078-8242 (Print), ISSN: 3078-2309 (Online) | Vol. 9, No. 2, 2026

Heat mass Transfer Coupling Model for Cylindrical Herbal Medicines under Variable-Property Hot-air Drying

Guanxi Yang *

School of Mechanical Engineering, Tianjin University of Science and Technology, Tianjin, 300457, China

* **Corresponding author**: (Email: ygx093534@163.com)

Abstract: Aiming at the hot air constant temperature drying process of cylindrical Chinese herbal medicines, a one dimensional unsteady heat mass transfer coupling mathematical model in cylindrical coordinates is established considering thermophysical parameters varying with moisture content and temperature. The temperature and moisture content distributions obtained from pre heating simulation are taken as the initial drying field. Boundary conditions coupling convective heat transfer, convective mass transfer and water evaporation latent heat are imposed on the outer surface of herbal material. The finite volume fully implicit difference method combined with Picard iteration is adopted to solve the strongly nonlinear equations, and the Thomas algorithm is used for tridiagonal linear systems. The spatiotemporal distributions of radial temperature and dry basis moisture content within herbal samples in the first 3 h of constant temperature drying are obtained by simulation. The results show that the material temperature approaches hot air temperature in about 2 h, while restricted by internal water diffusion, the dry basis moisture content at the cylinder axis still reaches 1.4541 kg/kg after 3 h drying. The dehydration front gradually propagates from the surface toward the core. The proposed model can reproduce the heat mass transfer evolution during drying, and provides theoretical support for parameter optimization of hot air drying technology for Chinese herbal medicines.

Keywords: Chinese herbal medicine, Hot air drying, Heat mass transfer coupling, Variable thermophysical property, Finite volume method.

1. Introduction

Hot-air drying acts as a key primary-processing procedure for Chinese herbal medicines. Drying parameters directly determine finished-product quality, energy consumption and total processing cycle [1-2]. Cylindrical rhizome herbal materials are typical porous media, where heat conduction and moisture diffusion evolve simultaneously and are strongly coupled during drying. Thermophysical properties of materials vary significantly with moisture content. Pure experimental trial-and-error for process debugging consumes substantial manpower and material resources [3-4]. Numerical heat-mass-transfer-coupled models can reveal the spatiotemporal evolution of internal temperature and moisture fields, providing theoretical support for process-parameter optimization and benefiting standardized processing of herbal medicines [5-6].

Current research on porous-material drying falls mainly into two categories: empirical kinetic models and physics-driven coupled models [7-8]. A large number of studies adopt empirical kinetic equations such as Page and Modified-Page to fit drying experimental curves, which can rapidly obtain macroscopic drying rates but fail to resolve radial field distributions inside materials [9-10]. Some literature establishes one- or multi-dimensional heat-mass-transfer models; nevertheless, many of them treat thermophysical parameters as constants and ignore moisture-dependent variations of thermal conductivity and diffusion coefficients. Several existing studies directly take hot-air temperature as the surface boundary condition, without fully considering surface energy coupling induced by evaporation latent heat. Hence they cannot accurately reproduce the table-to-core dehydration evolution inside cylindrical herbal materials.

To address the above research gaps, this paper establishes a one-dimensional unsteady heat-mass-transfer coupled model with variable thermophysical properties for cylindrical herbal medicines. Temperature and moisture-content distributions output from pre-heating simulation are adopted as initial drying fields. Coupled boundary conditions for convective heat transfer, convective mass transfer and evaporation latent heat are imposed on the outer surface. The finite-volume fully-implicit difference scheme combined with Picard iteration is employed to solve strongly-nonlinear equations, and the Thomas algorithm is applied for tridiagonal systems. Spatiotemporal radial distributions of temperature and dry-basis moisture content within materials during the first 3 h of constant-temperature drying are simulated, and field-evolution rules are revealed. This work provides theoretical references for hot-air-drying process optimization of cylindrical rhizome Chinese herbal medicines.

2. Methodology

2.1. Modeling of Heat Transfer and Moisture Diffusion

A one-dimensional unsteady heat transfer equation and moisture diffusion equation are established in cylindrical coordinates. Governing equation for temperature field:

$$\rho(C)\cdot c_p(C)\cdot\frac{\partial T}{\partial t}=\frac{1}{r}\frac{\partial}{\partial r}\left(k(C)\cdot r\cdot\frac{\partial T}{\partial r}\right) \quad (1)$$

Where: $T(r,t)$ denotes the material temperature at radial position r at time t (°C); $\rho(C)$ is the density of wet material (kg/m³); $c_p(C)$ is the constant-pressure specific heat capacity of wet material (J/(kg·K)); $k(C)$ is the thermal conductivity

of material (W/(m·K)). The governing equation for moisture content field is derived from Fick's second law:

$$\frac{\partial C}{\partial t} = \frac{1}{r}\frac{\partial}{\partial r}\left(D(C,T)\cdot r\cdot\frac{\partial C}{\partial r}\right) \quad (2)$$

Where: $C(r,t)$ denotes the dry-basis moisture content at radial position r at time t (kg/kg); $D(C,T)$ is the effective moisture diffusion coefficient (m^2/s), which depends on both moisture content and temperature and exhibits strong nonlinear characteristics.

During drying, the variation range of herbal moisture content is significantly larger than that in the preheating stage. Changes in moisture content alter thermophysical properties of the material, while temperature modifies the moisture diffusion coefficient. The temperature field and moisture content field form a bidirectional strong coupling relationship, and the two equations must be solved simultaneously.

2.2. Thermophysical Properties

All thermophysical parameters are state functions of local moisture content and temperature, and their specific expressions are given as follows: (1) Wet material density:

$$\rho(C) = 650 + 128C \quad (3)$$

During drying, as internal moisture continuously migrates outward, the local moisture content of herbal material decreases, the material density at corresponding positions drops, which further changes local heat capacity and affects the rate of temperature variation. (2) Constant-pressure specific heat capacity:

$$c_p(C) = 1450 + \frac{2736C}{C+1} \quad (4)$$

The specific heat capacity of water is much higher than that of the solid matrix. Higher moisture content leads to larger overall specific heat capacity. This function is a nonlinearly increasing function: the specific heat capacity rises rapidly at low moisture content, while its growth gradually slows down and stabilizes when moisture content keeps increasing. In the drying process, the surface moisture content decreases rapidly, the material specific heat capacity reduces accordingly, and temperature changes more easily under the same heat input. (3) Thermal conductivity:

$$k(C) = 0.21 + \frac{0.38C}{C+1} \quad (5)$$

Water has stronger thermal conduction capacity than the solid matrix. Higher internal moisture content of the material yields better overall thermal performance. Thermal conductivity increases nonlinearly with moisture content. At low moisture content, thermal conductivity is highly sensitive to moisture variation; after moisture content rises to a certain level, the growth of thermal conductivity gradually flattens. At the initial drying stage, moisture on the herbal surface is lost rapidly, and the surface thermal conductivity drops quickly, hindering further heat transfer into the herbal interior. (4) Effective moisture diffusion coefficient:

$$D(C,T) = 2.4\times10^{-3}\cdot\exp\left(-\frac{0.45}{C}\right)\cdot\exp\left(-\frac{3850}{T+273.15}\right) \quad (6)$$

When the internal moisture content of the material is very low, water is tightly adsorbed by the solid matrix and migration hardly occurs. As temperature rises, molecular thermal motion intensifies and moisture diffusion capacity improves significantly.

2.3. Initial and Boundary Conditions

After 30 minutes of preheating, a stable radial temperature gradient and moisture distribution have formed inside the herbal sample. This non-uniform field is directly adopted as the initial state for the drying stage.

Initial Conditions. The starting time of drying simulation corresponds to the moment at the end of preheating. Different from the uniform initial state over the whole domain at the start of Problem, a radial temperature gradient (high outside and low inside) and a non-uniform moisture distribution with slight surface dehydration have already formed inside the herbal material. The full-field radial distributions of temperature and dry-basis moisture content solved in Problem are assigned as the initial field of this problem, realizing seamless connection between preheating and drying conditions. The expression of initial condition is:

$$\begin{cases} T(r,t=0) = T_{preheat}(r) \\ C(r,t=0) = C_{preheat}(r) \end{cases} 0 \le r \le R_0 \quad (7)$$

Where the herbal radius $R_0 = 0.02\text{m}$; $T_{preheat}(r)$ and $C_{preheat}(r)$ are the temperature and dry-basis moisture content at position r at the end of preheating, respectively.

After preheating, a temperature gradient (high outside and low inside) and moisture distribution with slight surface dehydration are established inside the herbal sample. This residual field can truly reflect the actual state of herbal material after preheating, conforming to the continuous processing procedure of preheating followed by drying, and effectively guarantee the continuity and accuracy of drying simulation.

Boundary Conditions. Axisymmetric boundary (r=0): The herbal sample has a regular cylindrical structure. The axis center is the geometric symmetry center, without radial flow and gradient transport phenomena. Therefore, the radial temperature gradient and moisture gradient are always zero, and there is no exchange or loss of heat flux and mass flux at the axis:

$$\left.\frac{\partial T}{\partial r}\right|_{r=0} = 0, \left.\frac{\partial C}{\partial r}\right|_{r=0} = 0 \quad (8)$$

Outer surface coupled boundary ($r=R_0$): The outer surface of herbal material serves as the interface for energy and mass exchange between material and hot-air environment. Unlike the physical process dominated by temperature rise and heat conduction in preheating, there exists a remarkable moisture content difference between the herbal surface and air during drying. Continuous surface evaporation phase change of moisture occurs, and energy loss caused by vaporization latent heat cannot be neglected. Hence, multiple effects including convective heat transfer, convective mass transfer and phase change heat consumption coexist on the outer surface.

Convective mass transfer boundary: Driven by moisture concentration gradient, all moisture diffused from the herbal interior to the surface is transferred to the hot-air environment by convection to complete drying and dehydration. According to the continuity conservation principle of interface mass flux, the internal diffusion flux equals the interface convective mass transfer flux:

$$-D\left.\frac{\partial C}{\partial r}\right|_{r=R_0} = h_m\cdot\left(C_{\text{surf}} - C_{e,\text{air}}\right) \quad (9)$$

Note: The temperature term in this empirical formula uses

thermodynamic Kelvin temperature, while the temperature obtained by simulation is in Celsius, so unit conversion is required when calculating diffusion coefficients.

This boundary indicates that when the moisture content on the herbal surface is higher than the equilibrium moisture content of air, moisture will continuously migrate from inside to outside, which is the core driving condition for the attenuation of material moisture content throughout the drying process.

Convective heat transfer coupled with evaporation latent heat boundary: The surface energy balance during drying must consider phase-change heat consumption. Not all heat input from hot-air convection is used for material temperature rise; most energy is consumed by vaporization latent heat of water evaporation, producing an obvious evaporative cooling effect. Based on the interface energy conservation law, the energy boundary condition coupled with phase-change loss is constructed:

$$-k\frac{\partial T}{\partial r}\Big|_{r=R_0} = h(T_{\text{air}} - T_{\text{surf}}) - L_v \cdot h_m \cdot (C_{\text{surf}} - C_{e,\text{air}}) \quad (10)$$

Parameter values: convective heat transfer coefficient $h = 25\,\text{W/(m}^2 \cdot \text{K)}$; hot-air temperature $T_{air} = 60°\text{C}$; convective mass transfer coefficient $h_m = 8 \times 10^{-7}\,\text{m/s}$; air equivalent equilibrium moisture content $C_{e,air} = 0.08\,\text{kg/kg}$; latent heat of water vaporization $L_v = 2.45 \times 10^6\,\text{J/kg}$.

Part of the heat brought to the herbal surface by hot air compensates for the thermal energy consumed by water evaporation, and the remaining part is transferred into the herbal interior through heat conduction, further changing the internal temperature distribution of the material.

3. Results

3.1. Numerical Results Analysis

The non-uniform radial distributions of temperature and moisture content obtained at the end of preheating in Problem are taken as the initial field to carry out 3-h coupled constant-temperature drying simulation. According to requirements, calculation results at radial positions of 0 cm, 0.5 cm, 1.0 cm, 1.5 cm and 2.0 cm are collected every 0.5 h. The time 0.0 h corresponds to the starting moment of constant-temperature drying, seamlessly connecting with the 1800 s calculation result of the preheating stage. The radial distributions of temperature and moisture concentration inside the herbal material at each moment are shown in Table 1 and Table 2.

Table 1. Herbal temperature within 3 hours (°C)

Time (h)	r=0 cm	r=0.5 cm	r=1.0 cm	r=1.5 cm	r=2.0 cm
0.5	49.9028	50.1704	50.9504	52.1787	53.7619
1.0	56.7547	56.8402	57.0889	57.4797	57.9821
1.5	58.9634	58.9892	59.0642	59.1823	59.3344
2.0	59.6412	59.6487	59.6705	59.7050	59.7495
2.5	59.8432	59.8453	59.8517	59.8618	59.8749
3.0	59.9051	59.9058	59.9078	59.9111	59.9154

It can be seen from Table 1 that 0.0 h is the starting moment of constant-temperature drying, inheriting the calculation results of the preheating stage. A radial temperature gradient exists inside the herbal material, with surface temperature higher than the axis temperature. Under 60°C hot air, the overall temperature of herbal material rises rapidly from 0 to 1.0 h, and the temperature at each position approaches the hot-air temperature. The temperature rise rate decreases significantly after 1.5 h. At drying time of 3.0 h, the axis temperature reaches 59.91°C and the surface temperature reaches 59.92°C. The radial temperature difference is basically eliminated, and the temperature over the whole domain of herbal material is close to the hot-air temperature. Heat has been fully transferred to the herbal core.

Table 2. Herbal moisture concentration within 3 hours (kg/kg)

Time (h)	r=0 cm	r=0.5 cm	r=1.0 cm	r=1.5 cm	r=2.0 cm
0.5	2.5109	2.4714	2.3194	2.0128	1.5958
1.0	2.2797	2.2239	2.0600	1.8019	1.4743
1.5	2.0202	1.9735	1.8373	1.6220	1.3393
2.0	1.8004	1.7611	1.6453	1.4583	1.2047
2.5	1.6147	1.5803	1.4780	1.3106	1.0790
3.0	1.4541	1.4232	1.3310	1.1788	0.9653

Combined with Table 2 to analyze the evolution law of moisture content: only the herbal surface undergoes obvious dehydration at the initial drying stage, while the moisture content at the core is still close to the initial value of 2.55 kg/kg. During drying, moisture diffuses from the interior to the surface and is then taken away by hot air. It presents the feature that surface moisture content decreases preferentially and dehydration gradually advances toward the axis. Restricted by moisture diffusion and transport, the variation of moisture content at the axis position has an obvious hysteresis. At drying time of 3.0 h, the surface moisture content of herbal material drops to 0.9653 kg/kg, the axis moisture content remains 1.4541 kg/kg, and the cross-sectional area weighted average moisture content is 1.2087 kg/kg.

Comparing the evolution results of temperature field and moisture field, the bidirectional coupling effect of the two fields can be observed. On one hand, hot-air heating raises the overall temperature of herbal material, increases the effective moisture diffusion coefficient, promotes the migration of internal moisture to the surface, and accelerates drying and dehydration rate. On the other hand, continuous reduction of moisture content on the herbal surface decreases the thermal conductivity of material, increases the thermal resistance for heat transfer to the core, and inhibits internal temperature rise to a certain extent. The simulated temperature and moisture distributions simultaneously reflect the above two competing physical effects, which are mutually consistent with the physical mechanism of the variable-property heat-mass transfer coupled model.

The drying target of this problem requires that the moisture content at all positions of herbal material is lower than 0.15 kg/kg. However, at drying time of 3 h, the axis moisture content of herbal material is still 1.4541 kg/kg, far higher than the threshold value.

3.2. Visualized Analysis

To further intuitively display the evolution characteristics of internal temperature field and moisture field of herbal material during constant-temperature drying, curves of temperature and moisture content at the axis and surface varying with drying time, distribution curves along the diameter at drying time of 3 h, time-space cloud maps of temperature-moisture content and radial contour cloud maps

at different moments are plotted respectively. The visualization results are shown in Figures 1–4.

Figure 1 shows the curves depicting the changes in the center and surface temperatures of the medicinal material, as well as its moisture content on a dry basis, with respect to drying time. At the initial drying stage, the surface temperature rises obviously faster than the axis temperature, and the temperature difference between them continuously shrinks over time. After about 2 h, the axis temperature and surface temperature are basically consistent. The surface moisture content is always lower than the axis moisture content. At the very beginning of drying, the surface moisture content presents a short slight rise due to rapid temperature rise promoting internal moisture migration toward the surface.

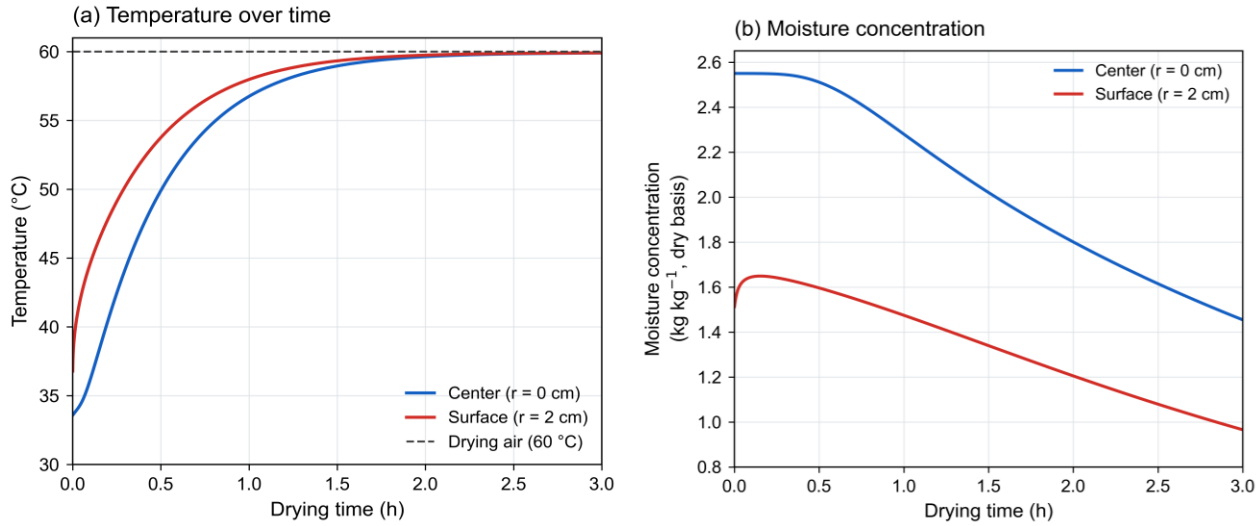

(a) Temperature-time curve (b) Humidity time-varying curve

Figure 1. Variation curves of temperature and dry-basis moisture concentration at herbal axis and surface with drying time

Figure 2 shows the distribution curves of temperature along the diameter and the moisture content on a dry basis of the medicinal material after 3 hours of drying. The overall temperature distribution shows a weak pattern of "low in the middle and high on both sides", but the axis-surface temperature difference is less than 0.01°C. The moisture content presents a parabolic distribution of high in the middle and low on both sides, with the core moisture content significantly higher than that on the surface.

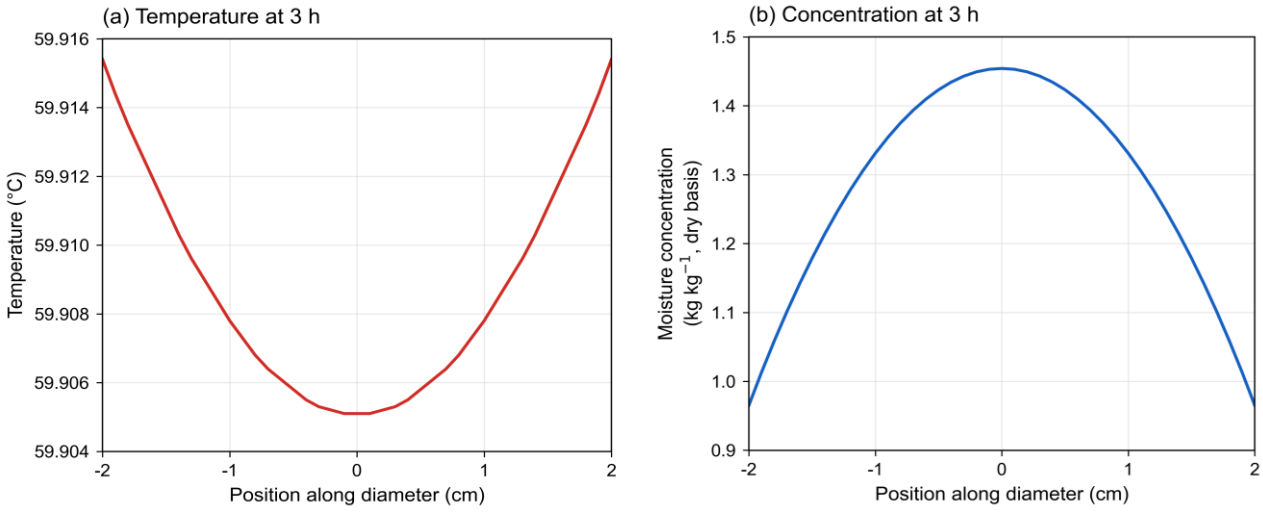

(a) Radial temperature distribution (b) Radial humidity distribution

Figure 2. Distribution curves of temperature and dry-basis moisture content of herbal material along the diameter at drying time of 3 h

Figure 3 shows the time-space evolution plots of the temperature and humidity fields during the drying process.

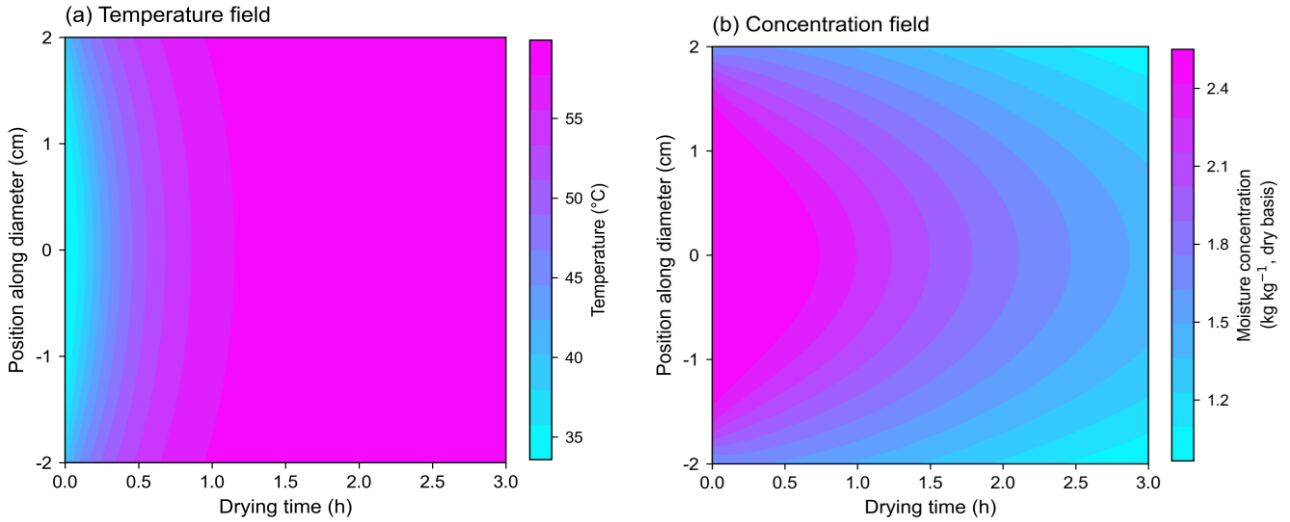

(a) Temperature field evolution (b) Evolution of the water concentration field

Figure 3. Time-space evolution cloud maps of temperature field and moisture concentration field during drying.

Figure 4 shows radial isocontour plots of temperature and water content across the cross-section of herbaceous plants at different time points. The temperature gradient gradually fades inward from the herbal surface, and the temperature over the whole domain quickly approaches the hot-air temperature. The moisture gradient slowly advances inward from the outer boundary, the dehydration region expands from the surface toward the axis, and the variation of core moisture content has an obvious hysteresis effect.

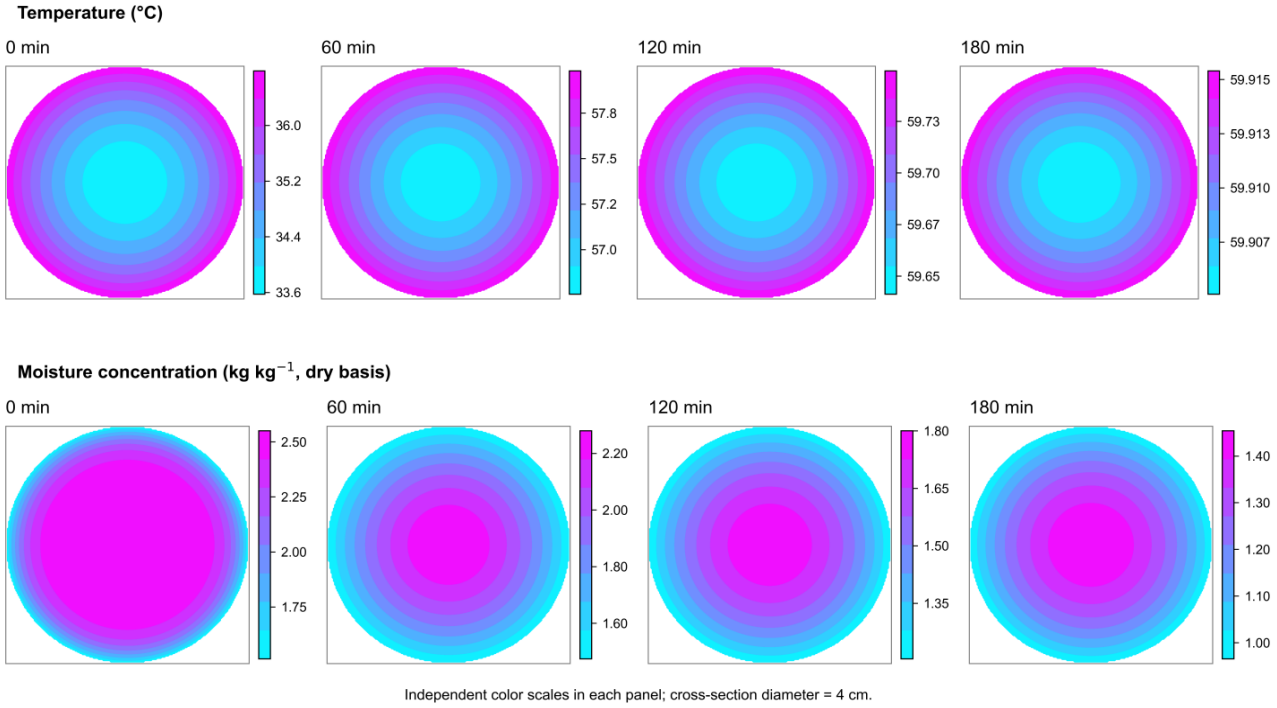

Figure 4. Radial contour cloud maps of temperature and moisture content on herbal cross-section at different moments

Coupling interaction exists between temperature field and moisture content field: temperature rise accelerates internal moisture diffusion, while property changes induced by surface dehydration hinder heat transfer inward to a certain degree. Combining quantitative table data and visualized image results, it can be concluded that 3 h constant-temperature drying cannot reduce the moisture content over the whole herbal domain to meet the drying standard, and longer drying duration is still required.

4. Conclusion

This paper establishes a one-dimensional unsteady heat-mass transfer coupled model with variable thermophysical properties for cylindrical herbal medicines under hot-air drying. Taking pre-heating simulation results as initial fields, the model solves temperature and dry-basis moisture content fields considering moisture-dependent thermophysical parameters and evaporation-latent-heat surface boundaries. Simulated by finite-volume fully-implicit difference, it reveals spatiotemporal evolution of radial temperature and moisture distribution. The model reproduces the coupling between heat conduction and moisture diffusion, and can be applied for mechanism analysis and pre-evaluation of hot-air drying processes for cylindrical rhizome herbal medicines.

Nevertheless, the present study still has limitation. Fixed convective heat-transfer and mass-transfer coefficients are used, and material shrinkage caused by water loss is not

considered. In future work, a moving-boundary shrinkage module will be integrated, and variable boundary coefficients will be adopted to reflect real hot-air flow characteristics. Furthermore, experimental data will be utilized to calibrate model parameters and improve prediction accuracy of the drying model.

References

[1] Borkakoti, S., Das, B., Ahmad, A., et al. (2026). Sustainable drying practices: Performance analysis of a single-slope solar greenhouse dryer in a humid subtropical climate for medicinal herbs. Arabian Journal for Science and Engineering, 1–17.

[2] Wang, B., Wang, S., & Ling, B. (2025). Recent advances in the drying of medicinal herb by novel physical field-based techniques: A review. Journal of Stored Products Research, 112, 102658.

[3] Yang, K., Han, H. T., Liu, J. Y., et al. (2024). Application progress of ultrasound in the production and processing of traditional Chinese herbal medicines. Ultrasonics Sonochemistry, 111, 107158.

[4] Vongpradubchai, S., Makul, N., & Rattanadecho, P. (2024). Novel microwave-assisted drying technique for Thai medicinal herbs utilizing an asymmetrical double-feed microwave/vacuum system. Engineered Science, 32.

[5] RA, S. H., WE, E. H., & KK, A. K. (2024). Effects of different methods of eggshells application on the productivity of sweet basil herb. Journal of Plant Nutrition, 47(11), 1763–1775.

[6] Li, S. Y., Qiu, R. X., Qi, R. Y., et al. (2024). Mechanisms of changes of active components in Chinese medicinal materials during drying: A review. China Journal of Chinese Materia Medica, 49(2), 315–324.

[7] Anfal, A., Hemanatha, J., PP, B., et al. (2022). Drying characteristics and quality analysis of medicinal herbs dried by an indirect solar dryer. Foods, 11(24), 4103.

[8] Eiji, G., Kayo, Y., & Masato, K. (2022). Challenge to the production of crude drugs by new technology "1st International Symposium on Kampo Medicine". Traditional & Kampo Medicine, 9(3), 196–197.

[9] Jean, G. (2022). Production of Chinese medicinal herbs in North America: Challenge and reconciliation. Chinese Medicine and Culture, 5(4), 234–240.

[10] Min, Z., Qiufang, C., Hong, W., et al. (2022). Comparison of protective effects of Shenmai injections produced by medicinal materials from different origins on cardiomyocytes. Evidence-Based Complementary and Alternative Medicine, 2022, 7205476.